Supplementary Materials
Accompanying 'The Frequency Dependence of Osmo-adaptation in *Saccharomyces cerevisiae*'
Mettetal *et al.*

MATERIALS AND METHODS

Strain

To construct DMY007, which we refer to as "wild type" in the text, the endogenous copy of Hog1 in the haploid BY4741 background strain was C-terminally tagged with yECitrine (YFP) using standard PCR integration (*S1*). Colony PCR was used to confirm this and all subsequent integrations. A C-terminal GFP fusion to Hog1 was previously shown to be functional (*S2*), and the response of Hog1-YFP matches that of Hog1-GFP (data not shown). To visualize the nucleus, PCR integration was used again to fuse mRFP1.3 (kind gift from E. O'Shea and R. Tsien) to the C-terminus of Nrd1, a nuclear protein involved in transcriptional termination and mRNA processing. Finally, a plasmid bearing the tet-inducible transcriptional activator rtTA under control of the *MYO2* promoter was integrated at the *LEU2* locus, and PCR was used to confirm a single integration. DMY008, the mutant strain used in this study, is identical to DMY007, except DMY008 expresses Pbs2 under the control of a TetO7 promoter. Specifically, we constructed a plasmid bearing two TetO7 promoters, one that drives CFP expression and the other that drives any gene of interest based on the primers used for PCR integration. For DMY008, this second TetO7 promoter drives Pbs2 expression.

Time-series Data Aquisition

The flow chamber is constructed as shown in Fig. S1. A channel is cut into an adhesive gasket with a thickness of 0.17 μm (Grace Biolabs), which is then sandwiched between a microscope slide and glass coverslip. Cells in log-phase growth from an overnight low-osmolarity culture are spun down and immobilized on the coverslip with Concanavalin A. Cells are then visualized with an inverted microscope (Nikon TE2000) and 100x objective. Media is constantly removed from the flow cell with a peristaltic pump (Pharmacia) coupled to a 125 ml media reservoir which dampens sudden changes in pressure. A computer-controlled valve selects the source of replacement media.

To measure the time the flow chamber takes to equilibrate, a small concentration of Rhodamine (Sigma) is added to the first media source. The average fluorescence of a region in the middle of the chamber visualized with a 4x objective is shown in Fig. S1. The rapid equilibration of the fluorescent signal indicates that the concentration of NaCl should also equilibrate in the chamber within 3-5 seconds.

In the experiments where new protein synthesis was inhibited, 100 μg/ml cycloheximide (Sigma) was added to both the low and high salt media sources of the

flow chambers. After cells were attached to the coverslip, the 0 M NaCl media was allowed to flow over the cells for 5-10 minutes after which we began to apply the square wave pulses of NaCl.

Data and Image Analysis

Fluorescence image analysis for determining $R(t)$ is performed with a custom Matlab (Mathworks) script. First, cell nuclei are found by thresholding the RFP images. The phase and YFP images are then used to find the cell boundary and cytoplasm which correspond to each nuclei found in the RFP image. Finally, cells whose cytoplasmic or nuclear volume suggested incorrect segmentation were rejected. The reported $R(t)$ is the population average taken over the approximately 50-300 cells observed in the microscope's field of view. Data fitting to obtain poles and other parameters is performed in Matlab by using an optimization algorithm to minimize the χ^2 error. The parameters and error bars for parameters in Table S1 are calculated by propagating experimental error bars through the fitting procedure.

SUPPLEMENTARY TEXT

Fourier Analysis

Once steady state oscillations have been reached, the output sine wave for driving frequency ω is represented through the formula (Fig. 2A):

$$R_\omega(t) = y_0(\omega) + A(\omega)\sin\left(\omega t + \phi(\omega)\right)$$

which has two parameters to characterize the oscillations, A and ϕ, and one parameter which characterizes the baseline, y_0. A and ϕ are represented through the absolute value and phase of the complex number $\tilde{R}(\omega)$ respectively. This complex number is calculated from the Fourier coefficient of the experimental data, $R_\omega(t)$, taken for stimuli with period T_0 using the relation:

$$\tilde{R}(\omega) = 2\int_{nT_0}^{(n+m)T_0} \frac{e^{-i\omega t} R_\omega(t)}{mT_0} dt\ .$$

The amplitude of the signal, defined as $A(\omega) = |\tilde{R}(\omega)|$, represents the half distance from the peak to the trough of the output sine wave. The phase parameter, $\phi(\omega)$, can be written implicitly as $\frac{\tilde{R}(\omega)}{|\tilde{R}(\omega)|} = e^{i(\phi(\omega)-\pi/2)}$. The parameter n is chosen so that the system is

allowed to approach steady state before calculating $\tilde{R}(\omega)$. The parameter *m*, which represents the number of periods over which we calculate the Fourier transform, is set to be at least two for periods less than 64 minutes. For periods greater than or equal to 64 minutes, we find the first period to be a good representation of the steady state oscillations and calculate $\tilde{R}(\omega)$ over this period alone.

Linear Time Invariant (LTI) Model

We write the linear input-output relationship in Fourier space as:

$$\tilde{Y}(\omega) = A_0 \frac{\prod_n (z_n + i\omega)}{\prod_n (p_n + i\omega)} \tilde{U}(\omega)$$

Here $\tilde{Y}(\omega)$ and $\tilde{U}(\omega)$ are the output and input Fourier spectra, respectively. The simplest such model from this class that accurately describes our data has three parameters $z_1 = 0$, and complex p_1 and p_2 yielding:

$$(p_1 + i\omega)(p_1 + i\omega)\tilde{Y}(\omega) = (i\omega)A_0\tilde{U}(\omega)$$

Applying the inverse Fourier transform produces a time derivative of *u* and *y* for each factor of $i\omega$ in the frequency-domain, which gives the following relationship in the time-domain:

$$\ddot{y} + (p_1 + p_2)\dot{y} + (p_1 p_2)y = A_0\dot{u}$$

A best-fit analysis (Fig. 2B) yields values for the wild-type of $A_o = 5.5\times10^{-3}$ M^{-1}, $p_1 = (0.0026 + 0.0038i)\,s^{-1}$ and $p_2 = (0.0026 - 0.0038i)\,s^{-1}$, and for the mutant (Pbs2 underexpression) strain of $A_o = 5.8\times10^{-3}$ M^{-1}, $p_1 = 1.2\times10^{-3}$ s^{-1}, and $p_2 = 1.6\times10^{-2}$ s^{-1}.

Non-linear Element Analysis

The LTI model predicts that the system will produce a negative output, *y*(*t*), in response to a dramatic reduction in the osmotic stimulus (large and negative $\dot{u}$). However, we observe that the amount of Hog1-YFP in the nucleus does not significantly decrease below the basal level, R_0, found in the absence of stimulus. We can easily augment the model and increase its accuracy in this scenario by passing the output of this dynamic linear equation, *y*(*t*), through a static non-linear element. This arrangement of a dynamic linear system followed by a static non-linear element is commonly referred to as a LN (Linear-Nonlinear) or Wiener System (*S3*). To determine the functional form of the non-

linearity, we plot the output of the linear element $y(t)$ calculated from Equation 2 versus the measured data points $R(t)$ in Fig. S3. The plot suggests that we relate the variable $y(t)$ to the observable $R(t)$ with a static transformation:

$$R_{\text{model}}(t) = f_{nl}(y(t)) + R_0$$

where R_0 = 1.237 is the basal response prior to osmotic stimuli, and the non-linear element $f_{nl}(y) = y(t) + |y(t)|$ acts as a rectifier to ensure that the response $R(t)$ is always greater than R_0. It is likely that this rectifying effect is due to the signaling elements upstream of Hog1, which only activate the downstream MAPK cascade in the presence of a positive osmotic pressure difference (hyper-osmotic shock).

We do find that the R_0 differs slightly depending on the strain, however the strain-to-strain variability was smaller than the experiment-to-experiment variability measured. For example, R_0 for the wild-type was found to be 1.237 with day-to-day variability of 0.05, while for the Pbs2 underexpression strain we find the value to be 1.226 with day-to-day variability of 0.02. When cells are stimulated with cycloheximide, on the other hand, the cells begin at T=0 with a basal nuclear Hog1 level similar to wild-type (roughly corresponding with the wild-type R_0). However, after several hours in cycloheximide, the basal nuclear Hog1 level is significantly higher, corresponding to R_0 = 1.33. One possible explanation for this observation is that the glycerol production rate decreases over time with the addition of cycloheximide (Fig. S6), and cells may have to weakly activate additional Hog1 in order to maintain their internal glycerol concentration.

While passing the system output through a non-linear element is intended to alter the response of the system, it does not affect the frequency response $A(\omega)$ and $\phi(\omega)$ measured from the linear system using the method we apply. This is true because the non-linearities will cause low frequency signals put into the non-linear element to 'mix' into and therefore affect measurements made at a higher frequency. However, the lowest frequency (i.e. the driving frequency) that propagates through our particular non-linear element will be unaffected by higher frequency components of the signal, and will propagate through the rectifier retaining both the phase and the amplitude. Because we obtain our measurements for $A(\omega)$ using the lowest frequency component of the input signal alone, the frequency response of the linear element we previously obtained remains valid independent of the static non-linear rectifier.

Mechanistic Model

We can write a general first order two-state model as a pair of differential equations with rate constants *a*, *b*, *c*, *d*, *e* and *f*.

$$\begin{bmatrix} \dot{X} \\ \dot{Y} \end{bmatrix} = \begin{bmatrix} a & b \\ c & d \end{bmatrix} \begin{bmatrix} X \\ Y \end{bmatrix} + \begin{bmatrix} e \\ f \end{bmatrix} u$$

We assume that one of the variables alone, namely *Y*, represents the observable Hog1 localization. This is similar to assuming that the dynamic variable *y* accounts for MAPK activity alone and the values we read out of the system are not influenced by other internal states or pathways. Therefore *X* is the variable representing the hidden state, and *u* represents the osmotic stimulus. When these equations are simplified to remove the hidden variable, *X*, we find a single second order differential equation in *Y*.

$$0 = (cb - ad)Y + (a + d)\dot{Y} - \ddot{Y} + (ce - af)u + f\dot{u}$$

When this equation is compared to the LTI model, we find that the relations $f = A_0$, $ce = aA_0$, and $c \neq 0$ must be true in order for the equations to be equivalent. Substituting these relations we obtain:

$$\begin{bmatrix} \dot{X} \\ \dot{Y} \end{bmatrix} = \begin{bmatrix} \frac{ce}{A_0} & b \\ c & d \end{bmatrix} \begin{bmatrix} X \\ Y \end{bmatrix} + \begin{bmatrix} e \\ A_0 \end{bmatrix} u = \begin{bmatrix} \frac{e}{A_0} & b \\ 1 & d \end{bmatrix} \begin{bmatrix} A_0 u + cX \\ Y \end{bmatrix}$$

Defining $y \equiv Y$, $x \equiv -cX$, $\alpha \equiv -\frac{ec}{A_0}$, $\beta \equiv -bc$, and $\gamma \equiv -d$ we can write these equations as:

$$\begin{bmatrix} \dot{x} \\ \dot{y} \end{bmatrix} = \begin{bmatrix} \alpha & \beta \\ 1 & -\gamma \end{bmatrix} \begin{bmatrix} A_0 u - x \\ y \end{bmatrix}$$

Comparing this relation with the LTI model, we can equate coefficients to obtain the relations:

$$\alpha + \gamma \equiv p_1 + p_2$$
$$\alpha\gamma + \beta \equiv p_1 p_2$$

and

$$p_1 = \frac{1}{2}\left((\alpha+\gamma)+\sqrt{(\alpha-\gamma)^2-4\beta}\right)$$
$$p_2 = \frac{1}{2}\left((\alpha+\gamma)-\sqrt{(\alpha-\gamma)^2-4\beta}\right)$$

Modeling the Mutant Strain

To model the mutant strain, we use Equation 1 from the main text with a simple modification, namely that the rate of activation of Hog1 is reduced due to the decreased concentration of the upstream kinase Pbs2:

$$\dot{y} = c(A_0 u - x) - \gamma y$$
$$\dot{x} = \alpha(A_0 u - x) + \beta y$$

In this equation, c represents the relative decrease in Hog1 activation compared to wild-type. We can define a new value of the y variable for the strain, y_{pbs2}:

$$y_{pbs2} = \frac{y}{c}$$

This allows us to rewrite the dynamic equations and the system output, *R*, as:

$$\dot{y}_{pbs2} = (A_0 u - x) - \gamma y_{pbs2}$$
$$\dot{x} = \alpha(A_0 u - x) + (c\beta) y_{pbs2}$$

$$R_{\text{model}}(t) = c f_{nl}(y_{pbs2}(t)) + R_0$$

From these equations, we can see two major differences from Equation 1 describing the wild-type cells. First, the parameter β is now multiplied by the factor *c*, reducing the feedback from *y* into *x*. Second, the response of the system is now scaled by *c*, reducing the amplitude of the signal output from the system. In other words, we can expect the mutant strain to exhibit a reduction in the output signal, characterized by A_0, as well as a reduction in MAPK dependent feedback, characterized by the parameter β, both by a similar amount.

Model Parameters

There is not enough information contained in the two dynamic parameters, p_1 and p_2, to determine α, β and γ for the wild-type or mutant strain alone. To resolve the ambiguity,

we fit the LTI model defined by Equation 1 along with the static nonlinear element to the step function $R(t)$, the $A(\omega)$, and $\phi(\omega)$ data for both the wild-type and Pbs2 underexpression strains simultaneously. This is done by minimizing the sum of χ^2 cost functions for each function in each strain. Since the signaling cascade is operating with a decreased strength we assume that the parameters A_0 and β vary between the wild-type and mutant strains while α and γ remain the same for the two strains. We break the symmetry in the definition of α and γ by noting that Hog1 still reaches maximal activity on the order of 100 s in a strain whose Fps1 channels have been modified and can no longer adapt rapidly to osmotic shocks (*S4*). Table S1 summarizes the parameters resulting from this fitting procedure (Fig. S7). We find that the mutant is characterized by an A_0 and β reduced from wild-type parameters by factors of (0.45 ± 0.03) and (0.24 ± 0.15) respectively.

Measurement of Glycerol Production Rates

We measured the rate of glycerol production in wild-type cells when stimulated with multiple pulses of 0.5 M NaCl (Similar to Fig. S5D). These experiments were conducted either in the absence or presence of 100 μg/ml cycloheximide (Sigma). Cells were grown overnight to log phase (OD_{600} between 0.5 and 1.0), and at 0, 60, 120, and 180 min cells were washed and resuspended in fresh minimal media containing no NaCl. Similarly, at 30, 90, and 150 minutes cells were washed and resuspended in fresh minimal media containing 0.5 M NaCl. While suspended in 0 M NaCl media, aliquots were taken every ten-minutes, immediately boiled for ten minutes and then spun at 13,000 rpm for 3 min. 20 μl of this supernatant was added to 0.8 ml of free glycerol reagent (Sigma). The absorbance at 540 nm was measured and normalized by the OD_{600} of the culture in order to obtain a total glycerol level relative to the number of cells present (Fig. S6A-B). The change in total glycerol levels over 20 minutes were then used to calculate the relative glycerol production rates (Fig. S6C). Cells stimulated in the absence of cycloheximide show an increase in glycerol production rate after each pulse, while cells stimulated in the presence of cycloheximide show the opposite trend.

SUPPLEMENTARY FIGURES

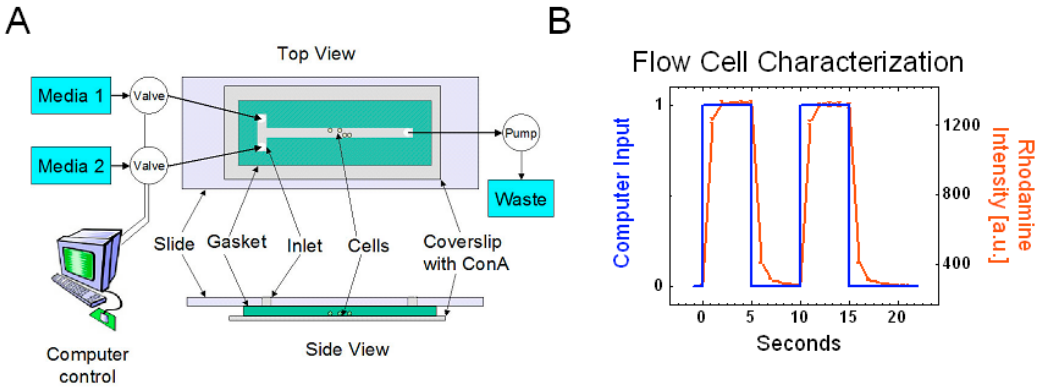

Fig. S1. (A) Schematic diagram of the flow-cell setup. A pump removes media from the flow chamber while a valve constantly selects from one of two fresh media sources. **(B)** Flow cell characterization indicates that the time-constant for complete media replacement in the flow chamber is significantly less than 10 seconds.

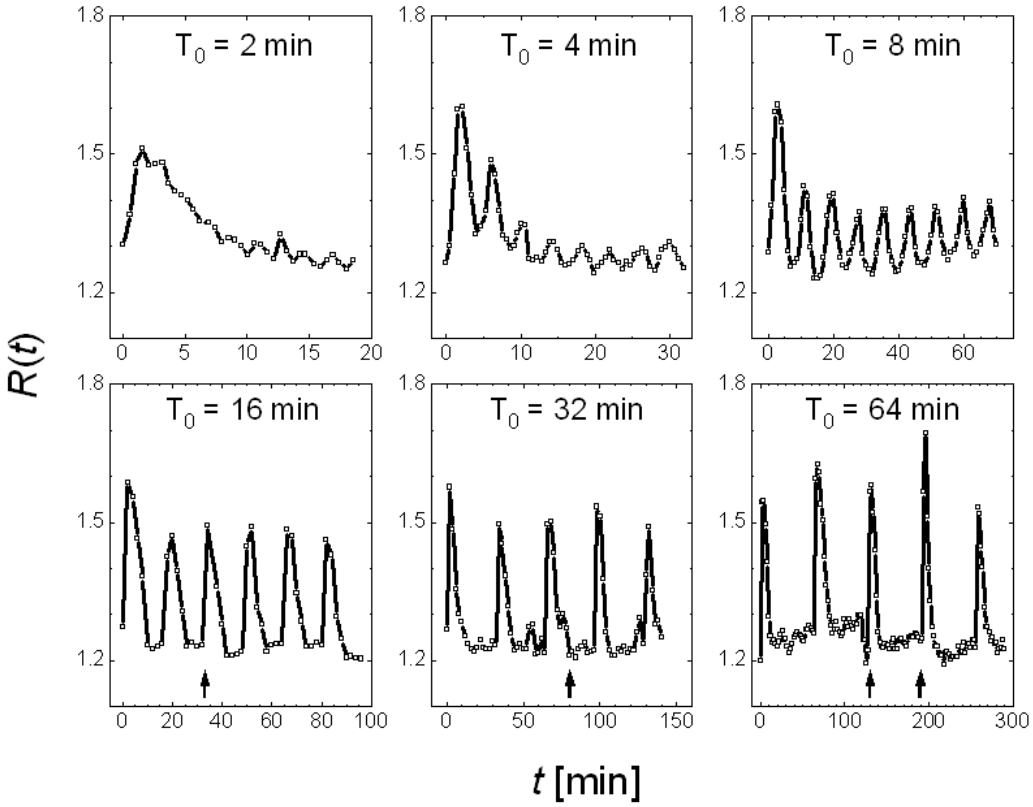

Fig. S2. Example $R(t)$ traces for the wild-type strain used to calculate the $A(\omega)$ and $\phi(\omega)$ data shown in Figs. 2B-C. Cells are stimulated with 0.2M square-wave pulses of NaCl with periods, T_0, ranging from 2 min to 64 min. Black arrows indicate a new field of view.

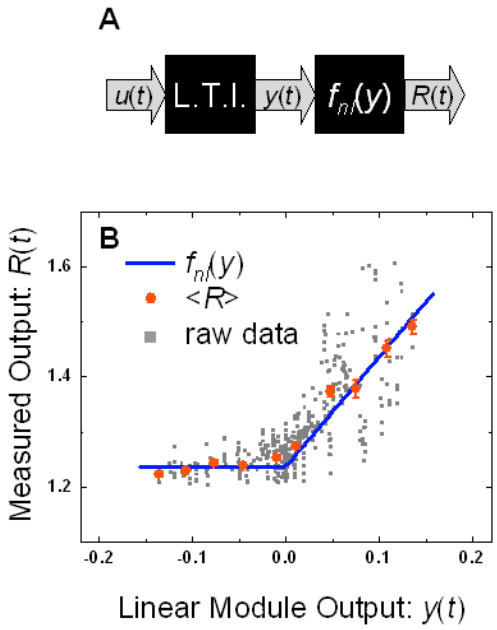

Fig. S3. (A) Diagram of the Wiener or LN setup of where the quantitative fitting of our linear model is enhanced by adding a static non-linear transfer element. **(B)** Measured model output plotted versus linear model prediction. The scatter plot shows that when the linear model predicts a negative response, the experimental system is near basal activity (gray boxes – individual points, red boxes - average). To account for this, we use a nonlinear element shown by the blue line.

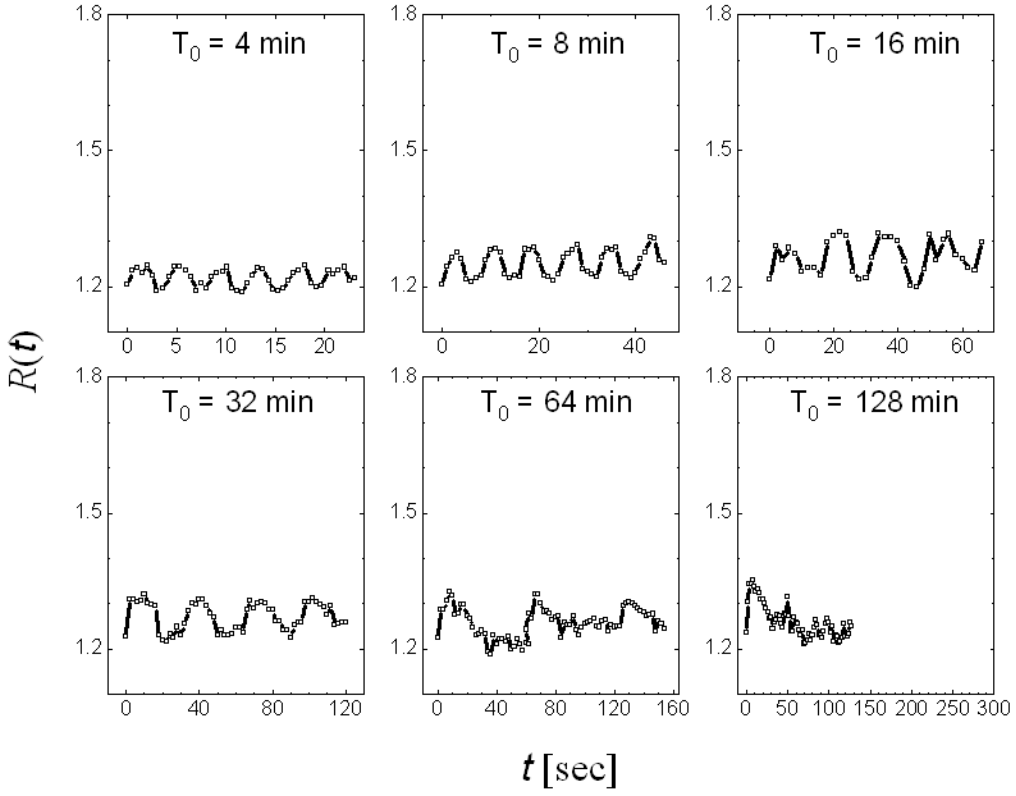

Fig. S4. Example $R(t)$ traces for the Pbs2 underexpression strain (DMY008) used to calculate the $A(\omega)$ and $\phi(\omega)$ data shown in Figs. 2B-C. Cells are stimulated with 0.2M square-wave pulses of NaCl with periods, T_0, ranging from 4 min to 128 min.

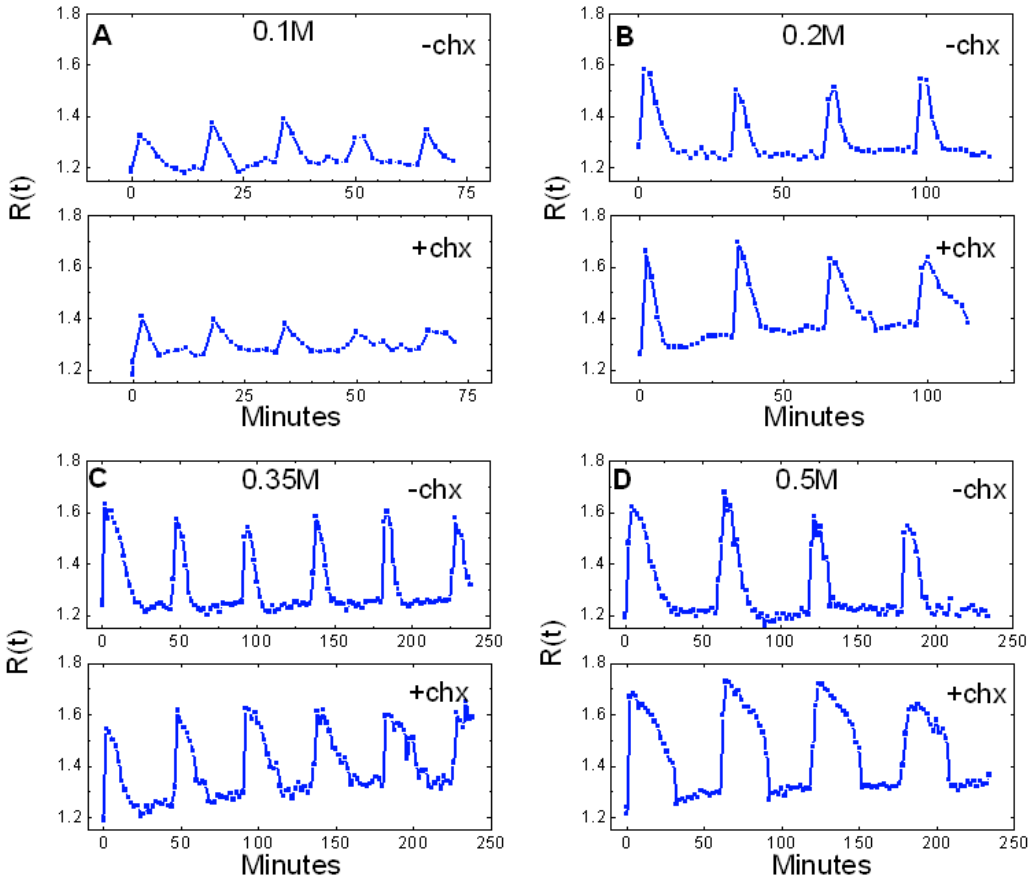

Fig. S5. Raw *R*(*t*) data for square wave pulses of **(A)** 0.1 M NaCl with 16 min period **(B)** 0.2 M NaCl with 30 min period **(C)** 0.35 M NaCl with 45 min period and **(D)** 0.5 M NaCl with 60 min period. Cells were stimulated at each concentration in the presence (+chx) and absence (-chx) of 100 μg/ml cycloheximide.

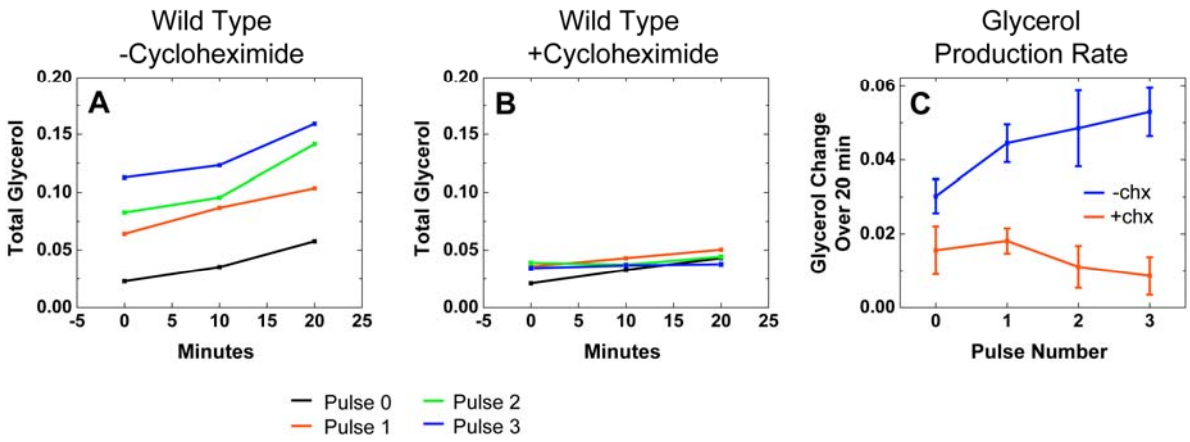

Fig. S6. (A) Glycerol levels measured in a population of wild-type cells after they have experienced zero, one, two, or three 30 minute long pulses of 0.5 M NaCl. **(B)** Glycerol levels in a population of wild-type cells stimulated by 30 minute pulses of 0.5 M NaCl in the presence of cycloheximide. **(C)** Change in total glycerol levels over a 20 min observation window was used to measure the rate of glycerol production in the population for both wild-type (blue) and wild-type + cycloheximide (red). The wild-type displays an increasing rate of glycerol production after each pulse, while the cells stimulated in the presence of cycloheximide display a slowly decreasing rate of glycerol production.

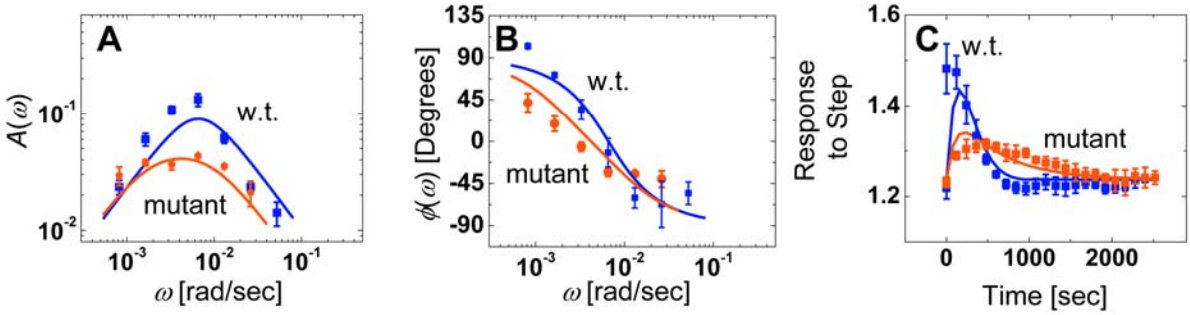

Fig. S7. Results of minimizing the χ^2 cost function over the **(A)** A(ω) **(B)** ϕ(ω) and **(C)** 0.2 M NaCl step response for the wild-type (blue) and mutant (red).

Supplementary Table S1. Estimates of Model Parameters

	wild type	*mutant*
A_0	$(8.0 \pm 0.3)\times10^{-3}$ (M NaCl)$^{-1}$	$(3.7 \pm 0.2)\times10^{-3}$ (M NaCl)$^{-1}$
β	$(3.4 \pm 0.5)\times10^{-5}$ s^{-1}	$(0.8 \pm 0.5)\times10^{-5}$ s^{-1}
γ	$(10.6 \pm 0.7)\times10^{-3}$ s^{-1}	$(10.6 \pm 0.7)\times10^{-3}$ s^{-1}
α	$(8.2 \pm 5.0)\times10^{-4}$ s^{-1}	$(8.2 \pm 5.0)\times10^{-4}$ s^{-1}

Supplementary References:

S1. Sheff, M.A. and K.S. Thorn, *Optimized cassettes for fluorescent protein tagging in Saccharomyces cerevisiae.* Yeast, 2004. **21**(8): p. 661-70.

S2. Ferrigno, P., et al., *Regulated nucleo/cytoplasmic exchange of HOG1 MAPK requires the importin beta homologs NMD5 and XPO1.* Embo J, 1998. **17**(19): p. 5606-14.

S3. Westwick, D.T., Kearney, R. E., *Identification of Nonlinear Physiological Systems*. 2003: IEEE Press.

S4. Klipp, E., et al., *Integrative model of the response of yeast to osmotic shock.* Nat Biotechnol, 2005. **23**(8): p. 975-82.